



PERGAMON

Journal of the Mechanics and Physics of Solids
49 (2001) 571–587

JOURNAL OF THE
MECHANICS AND
PHYSICS OF SOLIDS

www.elsevier.com/locate/jmps

Intersonic crack propagation in homogeneous media under shear-dominated loading: numerical analysis

Philippe H. Geubelle*, Dhirendra V. Kubair

Department of Aeronautical and Astronautical Engineering, Center for the Simulation of Advanced Rockets, University of Illinois at Urbana-Champaign, 306 Talbot Lab.; 104 South Wright Street, Urbana, IL 61801, USA

Received 25 January 2000; received in revised form 13 June 2000

Abstract

The transition from subsonic to intersonic propagation of a planar crack subjected to mixed-mode loading is investigated numerically using a spectral form of the elastodynamic boundary integral equations. The spontaneous motion of the propagating crack is simulated with the aid of a quasi-linear rate-independent cohesive failure model coupling normal and shear failure modes. It is observed that, when the loading amplitude is shear-dominated and represents a substantial fraction of the fracture plane strength, the dynamic crack undergoes a rapid transition to intersonic regime. In some cases, the transition takes place through the temporary creation ahead of the main crack of a secondary cohesive zone which quickly coalesces with the primary cohesive zone. In most cases, however, the subsonic-to-intersonic transition takes place through a rapid but smooth acceleration of the main cohesive failure zone. Intersonic crack propagation can be achieved under mixed-mode conditions when the shear component of the external loading is sufficiently large. However, under steady-state intersonic conditions, cohesive failure occurs exclusively in shear, even when the remote loading of the crack is of mixed-mode nature. © 2001 Elsevier Science Ltd. All rights reserved.

Keywords: A. Dynamic fracture; Intersonic crack propagation; B. Elastic material; C. Boundary integral equations

* Corresponding author. Tel.: +1-217-244-7648; fax: +1-217-244-0720.
E-mail address: geubelle@uiuc.edu (P.H. Geubelle).

1. Introduction

The issue of the limiting speed of a dynamic crack or fault propagating in a homogeneous medium has recently received a lot of attention in the solid mechanics, geophysics and physics communities. In the tensile (mode I) case, theoretical predictions based on the solution of a steadily propagating singular crack indicate that mode I cracks cannot exceed the Rayleigh wave speed c_R of the surrounding medium (Freund, 1990). For all super-Rayleigh crack speeds, including the intersonic regime, for which the crack speed v_c exceeds the shear wave speed c_s but remains below the dilatational wave speed c_d , the influx of energy into the crack tip becomes negative. In other terms, the propagating crack tip radiates energy instead of absorbing the energy needed to create free surfaces. This theoretical prediction of the limiting mode I crack speed has been confirmed experimentally by Washabaugh and Knauss (1994). By introducing a weak plane in a homogeneous brittle system, they prevented the appearance of the micro-cracking and branching processes which characterize the subsonic motion of mode I cracks and tend to limit their observed speed to approximately $0.5c_R$. As it propagated along the weaker plane, the crack quickly approached its theoretical limiting speed c_R .

The shear (mode II) situation is somewhat more complex. Direct observation of dynamic mode II crack propagation is very difficult to achieve due to the tendency of the crack to kink out of its original plane. In order to maintain planar crack motion under shear-dominated conditions, very high compressive loads are needed, such as those found in geophysical settings. Until recently, only indirect evidence of super-Rayleigh crack velocities has been collected in various earthquake events (Archuleta, 1982; Olsen et al., 1997). To achieve mode II crack propagation under laboratory conditions, Rosakis et al. (1999) have performed dynamic fracture experiments using shear-loaded Homalite specimen with a weak plane ahead of the initial crack. They observed that, when the loading amplitude exceeded a critical level, the crack rapidly accelerated to the intersonic regime, attaining speeds in the vicinity of $\sqrt{2}c_s$ and sometimes approaching the dilatational wave speed c_d . Inter-sonic crack speeds have also been observed by Ravi-Chandar and his co-workers (Ravi-Chandar et al., 2000; Zhu and Ravi-Chandar, 1999) using a slightly different setting in which a small groove is introduced in a shear-loaded PMMA specimen to prevent off-plane crack motion. Although the mechanisms of crack propagation observed in this second set of experiments was somewhat different and involved the creation of “echelon-type” micro-cracks, the global behavior of the shear crack, and, in particular, its attained speed were very similar to those observed by Rosakis and his co-workers.

At the analytical level, inter-sonic crack motion under mode II conditions has been studied both theoretically and numerically. The first numerical analysis of inter-sonic mode II crack motion is attributed to Andrews (1976) who used a 2D finite difference representation of the elastodynamic equations combined with a linear slip weakening model similar to that used in the present study. He showed that the appearance of a distinct failure zone ahead of the main crack was responsible for the subsonic-to-inter-sonic transition. Other numerical schemes have also been used to study inter-sonic crack motion under pure shear conditions: the boundary integral method (Das and Aki, 1977;

Andrews, 1985), molecular dynamics simulations (Abraham and Gao, 2000), and various forms of the finite element method (Johnson, 1990, 1992; Needleman, 1999).

The related theoretical studies have mostly focused on the steady-state intersonic motion of semi-infinite mode II crack or on the self-similar intersonic extension of a finite shear-loaded crack (Freund, 1979; Burrige et al., 1979; Broberg, 1989, 1995). Their findings can be summarized as follows: Firstly, just like in mode I situation, the subsonic super-Rayleigh range of crack speeds ($c_R < v_c < c_s$) is forbidden, since it corresponds to a negative energy release rate. Secondly, if a point-size process zone model is adopted, only one intersonic crack velocity ($\sqrt{2}c_s$) is possible, since the stress singularity characterizing the other intersonic crack velocities is less than $-\frac{1}{2}$, yielding a vanishing energy release rate. Thirdly, if a finite-size cohesive failure zone model is introduced, all intersonic crack speeds yield a finite value of the energy release rate and are therefore acceptable. The energy release rate is maximum for a crack speed in the vicinity of (but always superior to) $\sqrt{2}c_s$, with the location of the maximum depending on the cohesive model used and on the size of the cohesive zone. Finally, crack speeds below that for which the energy release rate is maximum are unstable, as the corresponding driving force decreases with v_c in that range.

In this paper we present a detailed numerical analysis of mode II and mixed-mode intersonic crack motion using a combination of a spectral boundary integral scheme and a simple rate-independent quasi-linear coupled cohesive failure model. In particular, we address the following outstanding issues: (1) How does the subsonic-to-intersonic transition take place? Is the creation of a secondary failure zone ahead of the main crack, as first shown by Andrews (1976), the only possible mechanism leading to intersonic crack motion, as conjectured by Burrige et al. (1979)? How can we describe the energetics of the transition? (2) What happens under mixed-mode conditions? Since only subsonic crack speeds are possible under tensile (mode I) conditions, how much shear dominance is required to achieve intersonic crack motion? Under what conditions does subsonic crack motion take place in the mixed-mode case? And how does the failure take place in the cohesive zone under steady-state and transient intersonic conditions?

The paper is organized as follows: in Section 2, we describe the model dynamic fracture problem and the numerical scheme used to simulate it. Then, we summarize and discuss the results of the pure-shear (Section 3) and mixed-mode (Section 4) problems.

2. Problem description and numerical scheme

The model plane strain dynamic fracture problem solved hereafter is schematically represented in Fig. 1. Two homogeneous linearly elastic half-spaces with identical properties are joined together along the plane $x_2 = 0$ and are subjected to a uniform mixed-mode loading amplitude τ^0 . As in the experiments performed by Rosakis et al. (1999), the specimen is made of Homalite, a brittle polymeric material with a Young's modulus $E = 5300$ MPa, Poisson's ratio $\nu = 0.35$ and density $\rho = 1230$ kg/m³, resulting in a dilatational wave speed $c_d = 2630$ m/s and a shear wave speed $c_s = 1263$ m/s under plane strain conditions. The amount of mode mixity is denoted by the angle

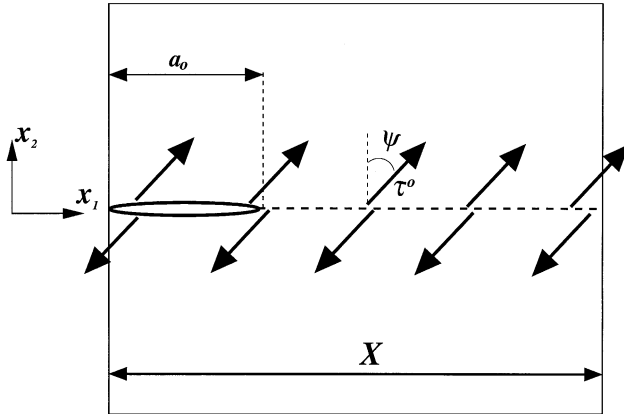


Fig. 1. Geometry of the model dynamic fracture problem.

ψ , with $\psi = 0$ and 90° corresponding to pure tensile (mode I) and shear (mode II) loading, respectively. We do not investigate in the present paper situations in which the domain is subjected to a compressive stress ($\psi > 90^\circ$) and where contact between crack faces becomes an issue. At time $t = 0$, a crack of length a_0 is introduced on the plane $x_2 = 0$ and starts to propagate spontaneously to the right, the left crack tip being held stationary.

As indicated earlier, we use the recently developed spectral scheme (Geubelle and Rice, 1995; Geubelle, 1997) to investigate this dynamic fracture problem. This numerical method has proven to be a very valuable tool to study various 2D and 3D fundamental dynamic fracture problems involving planar cracks or faults of arbitrary shapes embedded in an infinite medium and subjected to arbitrary dynamic loading conditions.

The spectral scheme, which basically consists in a special form of the elastodynamic boundary integral formulation, presents some major advantages over other more conventional numerical schemes such as the finite element and finite difference methods. Firstly, by focusing on quantities defined on the fracture plane, it allows for a very detailed study of the failure process taking place in the vicinity of the rapidly advancing crack front. Secondly, through the incorporation of various cohesive failure and frictional contact models, it allows for the simulation of a wide range of *spontaneous* dynamic fracture problems for which the crack motion is not prescribed a priori but is part of the solution itself. Finally, the spectral scheme is readily implemented on massively parallel computing platforms, allowing for the simulation of dynamic fracture problems at least two orders of magnitude larger than other methods (Breitenfeld and Geubelle, 2000).

Various forms of the spectral scheme have been developed over the past few years: homogeneous (Geubelle and Rice, 1995), bimaterial (Geubelle and Breitenfeld, 1997; Breitenfeld and Geubelle, 1998), viscoelastic (Geubelle et al., 1997; Danyluk et al., 1998) and replication-free (Cochard and Rice, 1997). For the mixed-mode

homogeneous elastodynamic problem at hand, the independent formulation proposed by Breitenfeld and Geubelle (1998) has been shown to be the most effective in terms of precision and stability, and is summarized in the remainder of this section.

As indicated earlier, the spectral scheme consists in a special form of the elastodynamic boundary integral relations between the traction stresses acting on the fracture plane and the resulting displacements. Unlike in the original formulation presented by Geubelle and Rice (1995) which was written in terms of the displacement jumps across the fracture plane, the independent version of the spectral scheme used hereafter basically solves for the elastodynamic responses of the two half spaces independently before applying the appropriate interface conditions. Let $u_\alpha(x_\gamma, t)$ and $\sigma_{\alpha\beta}(x_\gamma, t)$ ¹ denote the elastodynamic displacement and stress solution fields over the entire domain. Let $\tau_\alpha(x_1, t) = \sigma_{\alpha 2}(x_1, 0, t)$ be the traction stresses acting on the fracture plane $x_2 = 0$, and $u_\alpha^\pm = u_\alpha(x_1, 0^\pm, t)$, the in-plane displacements of the two half-space boundaries. The elastodynamic response of the two half spaces can be written as

$$\tau_\alpha(x_1, t) = \tau_\alpha^0(x_1, t) - V_{\alpha\beta} \frac{\partial u_\beta^\pm}{\partial t} + f_\alpha^\pm(x_1, t), \tag{1}$$

where τ_α^0 denotes the externally applied, possibly time- and space-dependent traction stresses acting on the fracture plane, i.e., the stresses that would be observed along $x_2=0$ if no crack were present. In the model problem investigated hereafter, $\tau_1^0 = \tau^0 \sin \psi$ and $\tau_2^0 = \tau^0 \cos \psi$, where τ^0 and ψ have been defined in Fig. 1. In Eq. (1), $V_{\alpha\beta}$ is a diagonal matrix containing material properties

$$V_{11} = \frac{\mu}{c_s}, \quad V_{22} = \frac{c_d \mu}{c_s c_s}, \tag{2}$$

with μ , c_d and c_s denoting the shear modulus and dilatational and shear wave speeds, respectively. The last term in (1), $f_\alpha^\pm(x_1, t)$, corresponds to the convolution term and, in the spectral scheme, is expressed in the spectral domain as a time convolution between its Fourier coefficients $F_\alpha^\pm(t; q)$ and the Fourier coefficients $U_\alpha^\pm(t; q)$ of the interface displacements as

$$\begin{aligned} F_1^\pm(t, Q) &= \pm \mu |q| \int_0^t H_{11}(|q|c_s t') U_1^\pm(t - t'; q) |q|c_s dt' \\ &\quad + i(2 - \eta) \mu q U_2^\pm(t; q) + i \mu q \int_0^t H_{12}(|q|c_s t') U_2^\pm(t - t'; q) |q|c_s dt', \\ F_2^\pm(t, q) &= \mp \mu |q| \int_0^t H_{22}(|q|c_s t') U_2^\pm(t - t'; q) |q|c_s dt' \\ &\quad + i(2 - \eta) \mu q U_1^\pm(t; q) - i \mu q \int_0^t H_{12}(|q|c_s t') U_1^\pm(t - t'; q) |q|c_s dt'. \end{aligned} \tag{3}$$

In (3), q denotes the spectral mode number, $\eta = c_d/c_s$ and i is the imaginary number. The expression of the convolution kernels $H_{\alpha\beta}$ can be found in Breitenfeld and Geubelle (1998).

¹ Greek indices take the values 1 and 2.

Details of the numerical implementation of the spectral scheme can be found elsewhere (Morrissey and Geubelle, 1997; Geubelle, 1997). For completeness purpose, let us simply indicate here that the time-stepping scheme is explicit and that the spatial discretization involves the introduction of a uniform grid over a portion X of the fracture plane, thereby defining the sampling points needed in the FFT computation of the Fourier coefficients. To complete the formulation and allow for the spontaneous propagation of the crack, a simple rate-independent coupled cohesive failure model is used, which relates the normal (τ_n^{str}) and shear (τ_s^{str}) strengths of Homalite along the plane $x_2 = 0$ to the displacement discontinuities $\delta_\alpha = u_\alpha^+ - u_\alpha^-$ across the fracture plane as

$$\tau_{n,s}^{\text{str}} = \tau_{n,s}^c \left\langle 1 - \sqrt{\left(\frac{\delta_1}{\delta_s^c}\right)^2 + \left(\frac{\delta_2}{\delta_n^c}\right)^2} \right\rangle, \quad (4)$$

where $\langle a \rangle = a$ if $a > 0$ and $= 0$ otherwise, τ_n^c and τ_s^c denote the intact tensile and shear strengths of the fracture plane, while δ_n^c and δ_s^c correspond to the critical values of the normal and shear crack opening displacements beyond which complete failure is achieved. In all the simulations presented hereafter, the tensile and shear strengths of the fracture plane are assumed to be equal ($\tau_n^c = \tau_s^c = \tau^c = 5$ MPa). The critical values of the normal (δ_n^c) and tangential (δ_s^c) crack opening displacements entering the coupled cohesive failure law (4) are also assumed to be equal ($\delta_n^c = \delta_s^c = \delta^c$). In other words, in the present study, the tensile and shear failure characteristics of the material on the fracture plane are assumed to be identical. To conclude this brief presentation of the numerical method, let us indicate that, in the simulations discussed in the remainder of this paper, a uniform grid involving 2048 sampling points has been used to discretize a portion $X = 1$ m of the fracture plane. Finer spatial discretizations with up to 8192 uniformly distributed sampling points have also been used to check for the spatial convergence of the numerical solution.

Special care has been taken to capture the failure process taking place in the cohesive zone by discretizing the latter with at least 10 grid points. The time step Δt used in the explicit time marching scheme has been chosen as $0.4\Delta x/c_s$, with Δx denoting the spacing between the sampling points defined on the fracture plane.

3. Intersonic crack propagation under pure shear (mode II) loading

We start by revisiting the pure mode II situation ($\psi = 90^\circ$), first addressed numerically by Andrews (1976) in a somewhat similar setting using a finite difference scheme. By varying the loading amplitude τ^0 and the cohesive failure energy through the value of the critical crack opening displacement in shear δ^c , with the shear strength τ^c fixed at 5 MPa, a range of crack propagation behaviors is observed. Three representative cases labeled a to c are shown in Fig. 2, which presents the evolution of the locations of the cohesive zone tip (dashed curves) and crack tip (solid curves). For a low value of τ^0/τ^c ($\tau^0/\tau^c = 0.51$ — case a), the crack propagates subsonically and, because of the continuous influx of energy into the crack tip region, the crack speed asymptotically approaches the Rayleigh wave speed $c_R = 0.934c_s$. When the loading level is further

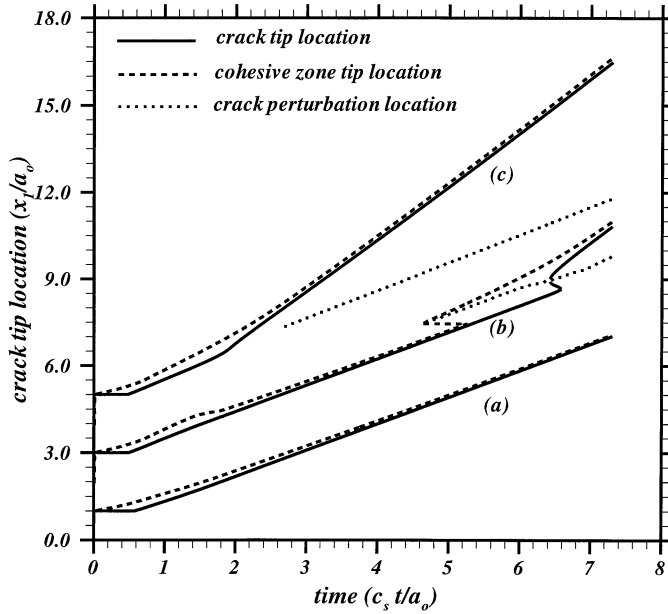


Fig. 2. Location of the tip of the cohesive zone (dashed curves) and of the crack (solid curves) in mode II case with $\delta^c/a_0 = 6.4 \times 10^{-4}$, for three values of the applied load amplitude τ^0 : for $\tau^0/\tau^c = 0.51$ (case a), the crack propagates subsonically; for $\tau^0/\tau^c = 0.55$ (case b) and $\tau^0/\tau^c = 0.57$ (case c), intersonic crack propagation is achieved. To avoid overlapping, the curves associated with cases b and c have been shifted vertically by $2a_0$ and $4a_0$, respectively. The dotted curves appearing for the two intersonic cases denote the location of the crack face Rayleigh wave perturbation shown in Fig. 3.

increased to $\tau^0/\tau^c = 0.55$ (case b), a transition is observed in the crack propagation behavior: ahead of the crack, a distinct cohesive failure zone develops temporarily and quickly merges with the main cohesive zone. At that point, the cohesive zone tip, followed, a little later, by the crack tip, starts to propagate intersonically and approaches a quasi-steady-state regime with a speed approximately equal to $1.9c_s$. The transition from subsonic to intersonic regime does not, however, always take place through the temporary creation of a distinct cohesive zone ahead of the main crack. In most cases, this transition takes place more smoothly as illustrated by case c in Fig. 2 corresponding to $\tau^0/\tau^c = 0.57$. In other words, in most cases, the crack crosses the forbidden ($c_R < v_c < c_s$) and unstable ($c_s < v_c < \sqrt{2}c_s$) zones through a rapid but smooth acceleration. This crack propagation behavior is consistently observed in our simulations and *does not* seem to be associated with the chosen discretization, as was suggested by Broberg (1995).

To help visualize the failure process involved in the subsonic-to-intersonic transition, snapshots of the shear displacement jump distribution $\delta_1(x_1, t)$ are presented for $\tau^0/\tau^c = 0.55$ (case b) in Fig. 3. The temporary appearance of a distinct cohesive zone ahead of the main crack and its coalescence with the main cohesive zone are clearly visible. Note also the presence of a perturbation propagating along the crack faces. This perturbation

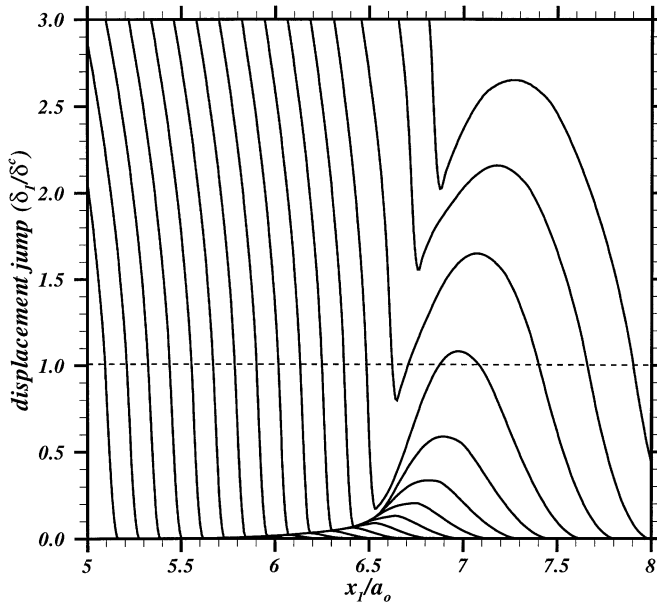


Fig. 3. Evolution of the crack opening in shear for the dynamically propagating mode II crack for case b ($\delta^c/a_0 = 6.4 \times 10^{-4}$ and $\tau^0/\tau^c = 0.55$). The curves are separated by a constant time interval equal to $c_s \Delta t/a_0 = 0.65$. The figure illustrates the appearance of a secondary cohesive zone and crack and its coalescence with the main crack. It also shows the crack face perturbation associated with the subsonic-to-intersonic transition.

is created at the crack tip when the intersonic transition takes place. It then propagates to the right at the Rayleigh wave speed, trailing the now intersonic shear crack, as indicated by the dotted curves in Fig. 2. This perturbation is present in all intersonic situations simulated in the present study.

Further illustrating the failure process, Fig. 4 presents the evolution of the shear traction stress τ_1 for four points located in the path of the dynamically advancing mode II crack. The first one (A) is located in the subsonic region ($x_1/a_0 = 4.8$), the second (B) and third (C) in the region where the transition takes place ($x_1/a_0 = 6.4$ and 6.8), respectively, and the last (D) in the region where quasi-steady-state intersonic conditions are achieved ($x_1/a_0 = 8.0$). The figure clearly illustrates the process leading to the creation of the secondary failure zone ahead of the main crack. As the crack approaches, the shear stress does not increase monotonically, but reaches a local maximum ahead of the tip of the primary cohesive zone (curve A). As long as the stress value associated with the local extremum remains below the strength of the fracture plane, the crack propagates subsonically. At some point (B), however, the local maximum reaches the critical stress value τ^c , thereby initiating the creation of the secondary cohesive zone. As the latter coalesces with the main crack, the local stress maximum progressively disappears (curve C), leading to the fully developed intersonic

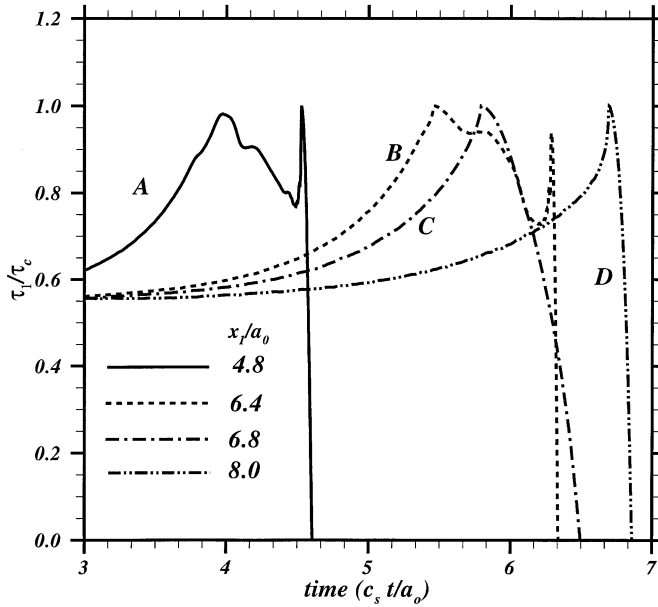


Fig. 4. Evolution of the shear traction stress τ_1 computed at four points located in the path of mode II crack. The loading condition corresponds to case b in Fig. 2.

conditions (curve D) for which the shear stress recovers a more conventional profile in the vicinity of the approaching crack.

The transition can also be studied from an energetic point of view through the evolution of the cohesive energy rate \dot{E} defined as

$$\dot{E}(t) = \int_{L_c(t)} \tau_s^{\text{str}}(x_1, t) \dot{\delta}_1(x_1, t) dx_1, \tag{5}$$

where $L_c(t)$ denotes the cohesive zone length at time t . The results corresponding to the two intersonic cases presented in Fig. 2 (cases b and c) are shown in Fig. 5, together with the evolution of the crack tip speed v_c . For case c characterized by a smooth transition from subsonic to intersonic regimes, the energy rate dissipated in the cohesive failure process undergoes a sharp but monotonic increase, including the crack velocity regime $c_R < v_c < c_s$, that is forbidden in the steady-state case. For the more unstable case (case b), the creation and coalescence of a second cohesive zone ahead of the main crack is associated with a sharp spike in dissipated cohesive energy rate. Note that the difference between the normalized \dot{E} and v_c curves denotes the contribution of the transient effects on the energetics of the cohesive failure process, since, under steady-state conditions, $\dot{E} = v_c G_c$, where $G_c = \tau^c \delta^c / 2$ denotes the fracture toughness of the material ahead of the crack.

In addition to that of the applied load level τ^0 , the effect of the toughness of the fracture plane on the propagation behavior of mode II crack has also been

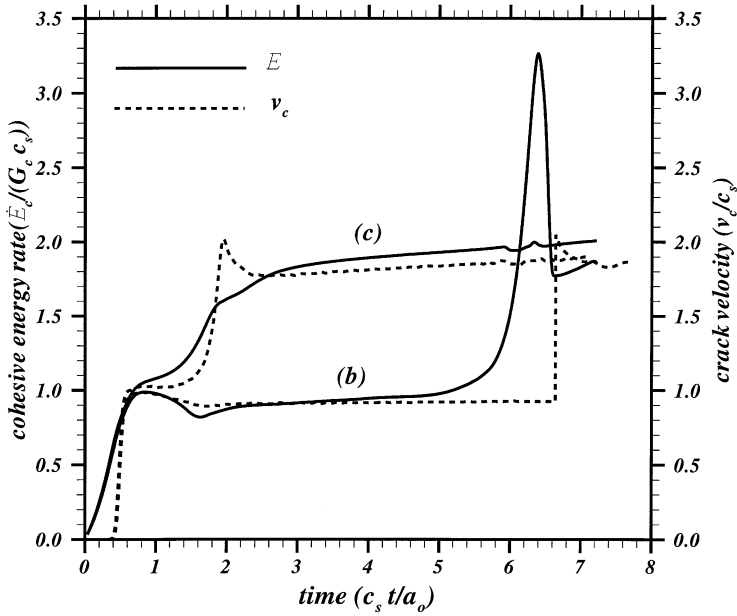


Fig. 5. Evolution of the rate of energy dissipated in the cohesive failure process (solid curves) and of the speed of the crack tip (dotted curves) for the two intersonic cases (cases b and c) shown in Fig. 2.

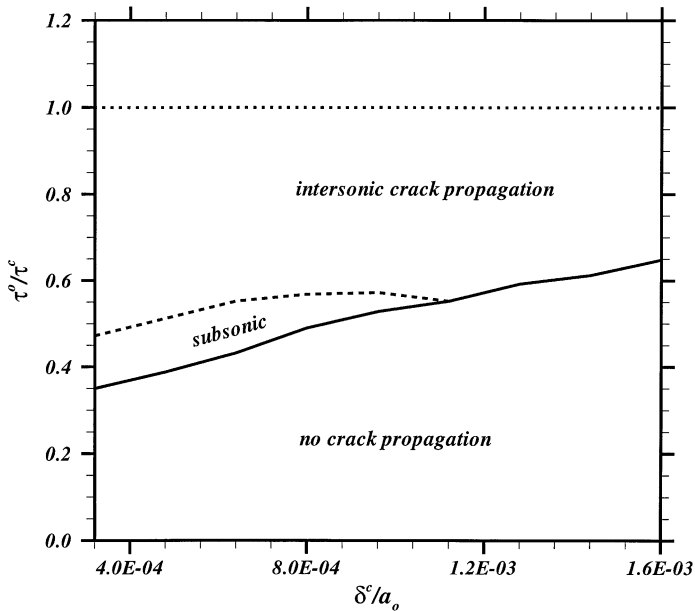


Fig. 6. Subsonic/intersonic map for mode II case, summarizing the effect of the loading amplitude τ^0 and of the fracture toughness (through the variation of the critical shear displacement δ^c) on the propagation regime of the dynamic crack. The solid curve denotes the upper bound of the non-propagating crack regime, while the dashed curve corresponds to the lower bound of the intersonic regime.

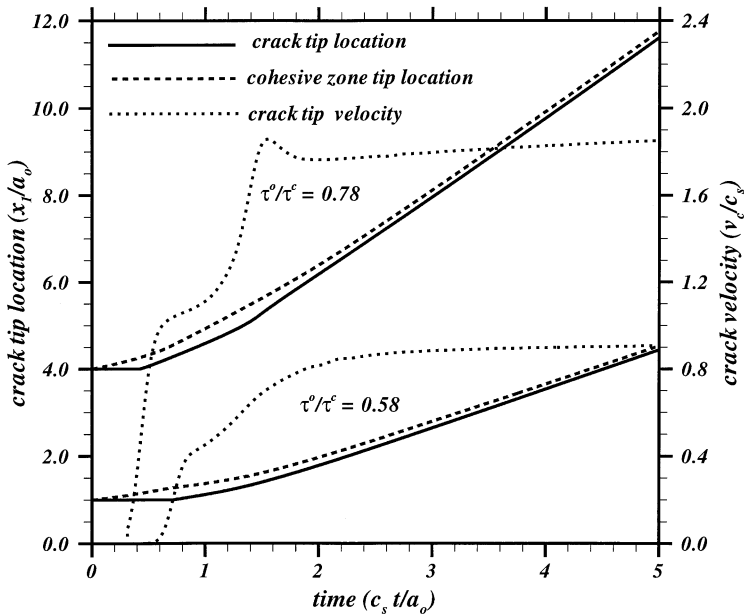


Fig. 7. Location of the cohesive zone tip (dashed curves) and of the crack tip (solid curves) for a mixed-mode case ($\psi = 50^\circ$ and $\delta^c/a_0 = 6.4 \times 10^{-4}$): for a low loading level ($\tau^0/\tau^c = 0.58$), the crack propagates subsonically; for higher loading values ($\tau^0/\tau^c = 0.78$), intersonic crack motion is observed as further indicated by the evolution of the crack tip velocity (dotted curves). For clarity, the crack and cohesive zone tip curves corresponding to the case $\tau^0/\tau^c = 0.78$ have been shifted vertically by $3a_0$.

systematically investigated by varying the critical value δ^c of the displacement jump. The results are summarized in Fig. 6, which illustrates the extent of the no-propagation, subsonic and intersonic regions on the (τ^0, δ^c) plane for mode II case. For low values of the fracture toughness, subsonic crack propagation can be achieved for intermediate values of the shear loading. When τ^0 exceeds a critical value, intersonic crack propagation is observed, as indicated earlier. For higher values of the fracture toughness, no subsonic regime is obtained and the crack only propagates intersonically. It is, however, important to note at this point that higher values of the fracture toughness would render planar crack propagation harder to achieve as the shear-loaded crack would have the tendency to kink out of its original plane. Let us note finally that the critical value of the applied load τ^0 needed to initiate intersonic crack motion is weakly dependent on the fracture toughness, and is of the order of $0.5\tau^c$.

4. Inter-sonic crack propagation under mixed-mode loading

We now turn our attention to the issue of intersonic crack propagation under mixed-mode conditions ($0^\circ < \psi < 90^\circ$). Of special interest here is the detailed study of the

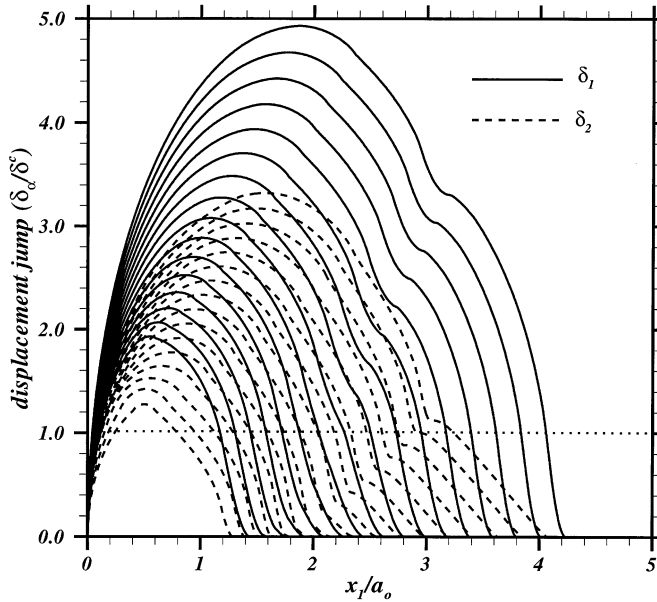


Fig. 8. Normalized crack opening profiles for the mixed-mode intersonic case shown in Fig. 7. The shear opening is denoted by solid curves, the normal opening by dotted curves. The displacement jump distributions are separated by a constant time interval equal to $c_s \Delta t / a_0 = 0.65$.

transition between mode I situation for which only subsonic crack motion has been shown to be possible, and mode II situation examined in the previous section, for which intersonic motion has been shown to exist for a limited range of loading conditions. Also, of interest in this section are the details of the failure process during the subsonic-to-intersonic transition and under fully established intersonic conditions.

Fig. 7 presents typical evolutions of the crack tip location and speed obtained for $\psi = 50^\circ$ and $\delta^c/a_0 = 6.4 \times 10^{-4}$, and for two loading levels, $\tau^0/\tau^c = 0.58$ and $\tau^0/\tau^c = 0.78$. The numerical solution for the mixed-mode case is very similar to mode II situation: for lower loading levels, subsonic crack motion is observed, while, for higher loading levels, the crack undergoes a rapid transition to the intersonic regime after propagating subsonically for a little while. In the majority of the mixed-mode cases, the transition takes place in a smooth fashion, reminiscent of case c of Fig. 2. In this particular case, the crack quickly reaches a speed approaching $1.9c_s$. The transition between subsonic and intersonic crack speeds is apparent in the relatively sudden increase in the spacing between normal (dotted curves) and tangential (solid curves) crack opening displacement profiles shown in Fig. 8. The aforementioned crack face Rayleigh wave perturbation associated with the transition is again clearly visible in the mixed-mode case. Fig. 8 also seems to indicate that, while both shear and tensile openings are observed in the cohesive zone in the subsonic regime, only shear failure is apparent in the

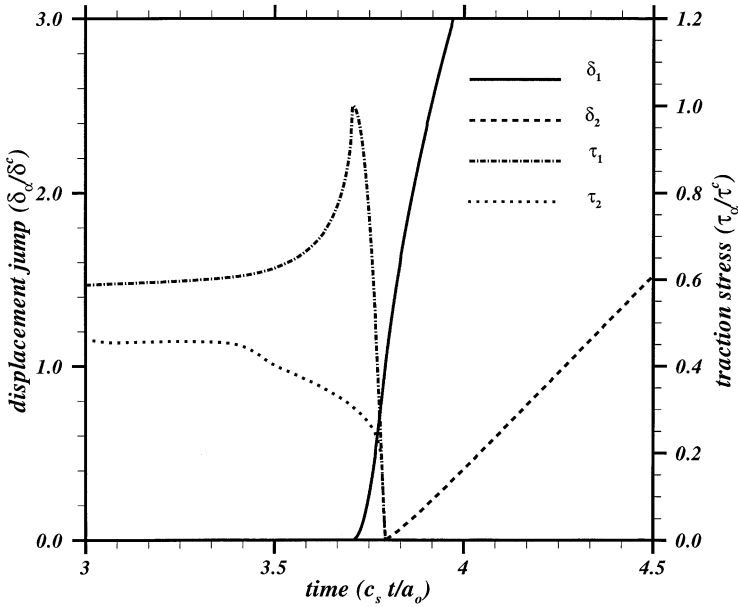


Fig. 9. Mixed-mode intersonic cohesive failure process: evolution of the normal (δ_2) and tangential (δ_1) displacement jumps and of the traction stresses (τ_x) computed at a point located in the path of an intersonically propagating mixed-mode crack (case $\tau^0/\tau^c = 0.78$ in Fig. 7). The figure illustrates that the failure takes place completely in shear and that normal opening is observed once the cohesive failure is completed.

cohesive zone in the fully established intersonic regime, and normal (tensile) opening of the crack is observed only outside of the cohesive failure zone. This fact is further illustrated in Fig. 9, which presents the evolution of the crack opening displacements and of the traction stresses for a point located in the path of the intersonically propagating mixed-mode crack ($x_1/a_0 = 6.4$). As the crack approaches, the shear stress τ_1 increases monotonically and reaches the critical value τ^c , thereby initiating the failure process. The tensile traction stress τ_2 remains well below the strength value in the major part of the cohesive zone. The crack opening δ_2 remains zero until the trailing edge of the cohesive zone passes by the point of observation, at which point the crack faces start to separate.

The failure takes place exclusively in shear, only under fully established quasi-steady-state intersonic conditions. Under subsonic conditions and during the transient subsonic-to-intersonic transition, a small amount of tensile cohesive failure is observed, as illustrated in Fig. 10, which presents the evolution of the rate of energy dissipated in the tensile (\dot{E}_2) and shear (\dot{E}_1) cohesive failure, defined as

$$\dot{E}_\alpha(t) = \int_{L_c(t)} \tau_\alpha^{\text{str}}(x_1, t) \dot{\delta}_\alpha(x_1, t) dx_1 \quad (\text{no sum on } \alpha). \tag{6}$$

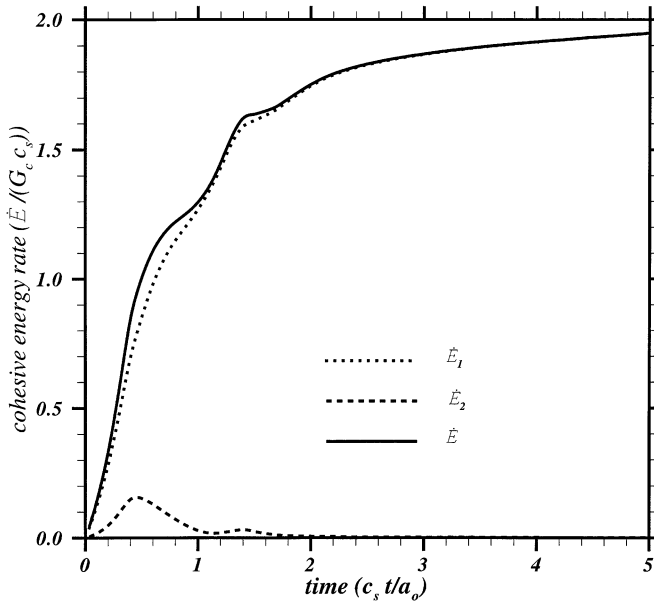


Fig. 10. Evolution of the rate of energy dissipated in tension (\dot{E}_2) and shear (\dot{E}_1) inside the cohesive zone as defined by (6). The solid curve corresponds to the total cohesive energy rate \dot{E} and emphasizes the predominance of the shear failure process especially as the quasi-steady-state intersonic conditions are achieved.

The total rate of energy dissipated in the cohesive failure model ($\dot{E} = \dot{E}_1 + \dot{E}_2$) is also shown, illustrating the predominant contribution of shear failure in the overall energy dissipation mechanism.

Finally, we present in Fig. 11 a summary of the effect of mode mixity (ψ), loading amplitude (τ^0) and fracture toughness (through the critical δ^c) on the crack propagation regime. As anticipated, in mode I case ($\psi = 0^\circ$), no intersonic region is observed for $\tau^0/\tau^c < 1$. This conclusion is still applicable for low values of the mode mixity parameter ($\psi \leq 40^\circ$) as the failure process remains mostly of tensile nature. As the mode mixity increases, shear failure becomes dominant and an intersonic regime zone progressively develops. The higher the shear component, the lower the loading level required to achieve intersonic crack propagation, the minimum value of τ^0 being achieved in the pure mode II case. Actually, since, as shown earlier, the cohesive failure process under steady-state intersonic condition takes place solely in shear even under mixed-mode condition, it is natural that the subsonic-to-intersonic transition is dictated by the value of the shear component on the applied load $\tau_1^0 = \tau^0 \sin \psi$. Indeed, when plotted in terms of τ_1^0 instead of τ^0 , the curves indicating the boundary of the intersonic region for the various mixity parameter ψ all collapse on the same curve, i.e., that corresponding to the pure mode II ($\psi = 90^\circ$) case.

To conclude this discussion of the mixed-mode case, let us indicate that, although the summary plot shown in Fig. 11 has been obtained for equal values of the fracture

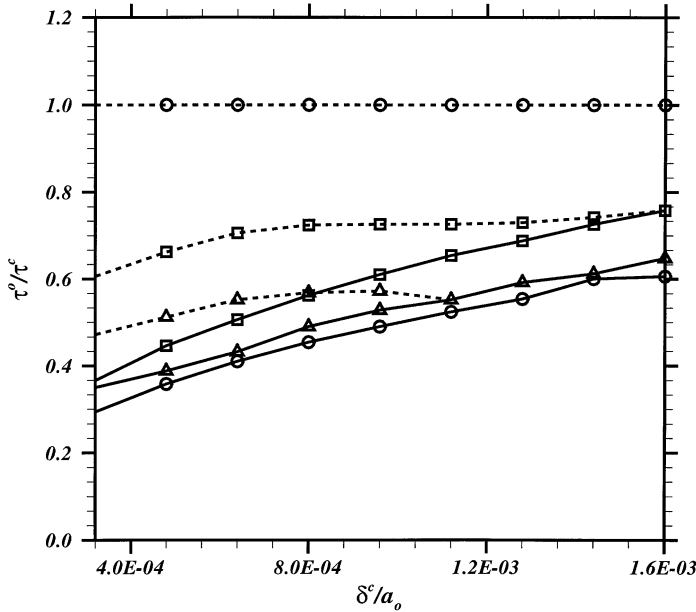


Fig. 11. Subsonic/intersonic map for the mixed-mode situation, for three values of the mode-mixity parameter ψ : $\psi = 0^\circ$ (circles), $\psi = 50^\circ$ (squares) and $\psi = 90^\circ$ (triangles). The solid and dashed curves have the same significance as in Fig. 6 and delimit the non-propagation, subsonic and intersonic regimes.

toughnesses and strengths in tension and shear, the main results of the mixed-mode study, i.e., the existence of an intersonic regime and the predominance of shear failure under intersonic condition, are still valid for other choices of the cohesive failure parameters.

5. Conclusion

A detailed numerical analysis of the subsonic-to-intersonic transition undergone by a planar crack subjected to shear-dominated loading conditions has been presented. The numerical scheme used in the analysis is based on spectral form of the boundary integral formulation and on a rate-independent cohesive model. Among the major results of the numerical study:

1. Inter-sonic crack propagation is possible for a wide range of loading conditions as long as the amplitude of the shear-dominated loading represents a substantial fraction of a strength of the fracture plane.
2. Even under mixed-mode conditions, failure in an inter-sonically propagating cohesive zone takes place in pure shear and tensile opening of the crack is observed only behind the crack tip.

3. In some cases, the subsonic-to-intersonic transition takes place through the creation of a secondary cohesive zone and possibly of a secondary crack, which eventually coalesce with the main advancing crack front. But, in most situations, the transition takes place through a sudden acceleration of the tip of the main cohesive zone.

Acknowledgements

Part of this work has been supported by the ASCI Center for the Simulation of Advanced Rockets funded by the U.S. Department of Energy through the University of California under subcontract number B341494. Some simulations have been performed on the NCSA Origin 2000.

References

- Abraham, F.E., Gao, H., 2000. How fast can cracks propagate? *Phys. Rev. Lett.* 84 (14) 3113–3116.
- Andrews, D.J., 1976. Rupture velocity of plane strain shear cracks. *J. Geophys. Res.* 81 (32), 5679–5687.
- Andrews, D.J., 1985. Dynamic plane-strain shear rupture with a slip-weakening friction law calculated by a boundary integral method. *Bull. Seismol. Soc. Am.* 75 (1), 1–21.
- Archuleta, R.J., 1982. Analysis of near source static and dynamic measurements from the 1979 Imperial Valley earthquake. *Bull. Seismol. Soc. Am.* 72, 1927–1956.
- Breitenfeld, M.S., Geubelle, P.H., 1998. Numerical analysis of dynamic debonding under 2D in-plane and 3D loading. *Int. J. Fract.* 93, 13–38.
- Breitenfeld, M.S., Geubelle, P.H., 2000. Parallel implementation of a spectral scheme for the simulation of 3D dynamic fracture events. *Int. J. High Performance Comput. Appl.* 14 (1), 26–38.
- Broberg, K.B., 1989. The near-tip field at high crack velocities. *Int. J. Fract.* 39, 1–13.
- Broberg, K.B., 1995. Interersonic mode II crack expansion. *Arch. Mech.* 47 (5), 859–871.
- Burridge, R., Conn, G., Freund, L.B., 1979. The stability of a rapid mode II shear crack with finite cohesive traction. *J. Geophys. Res.* 85 (B5), 2210–2222.
- Cochard, A., Rice, J.R., 1997. A spectral method for numerical elastodynamic fracture analysis without spatial replication of the rupture event. *J. Mech. Phys. Solids* 45 (8), 1393–1418.
- Danyluk, M.J., Geubelle, P.H., Hilton, H.H., 1998. 2D and 3D dynamic fracture in viscoelastic media. *Int. J. Solids Struct.* 35 (28–29), 3831–3853.
- Das, S., Aki, K., 1977. A numerical study of two-dimensional spontaneous rupture propagation. *Geophys. J. Roy. Astron. Soc.* 50, 643–668.
- Freund, L.B., 1979. The mechanics of dynamic shear crack propagation. *J. Geophys. Res.* 84, 2199–2209.
- Freund, L.B., 1990. *Dynamic Fracture Mechanics*. Cambridge University Press, Cambridge.
- Geubelle, P.H., 1997. A numerical method for elastic and viscoelastic dynamic fracture problems in homogeneous and bimaterial systems. *Comput. Mech.* 20 (1–2), 20–25.
- Geubelle, P.H., Breitenfeld, M.S., 1997. Numerical analysis of dynamic debonding under anti-plane shear loading. *Int. J. Fract.* 85, 265–282.
- Geubelle, P.H., Danyluk, M.J., Hilton, H.H., 1997. Dynamic mode III fracture in viscoelastic media. *Int. J. Solids Struct.* 35, 761–782.
- Geubelle, P.H., Rice, J.R., 1995. A spectral method for 3D elasto-dynamic fracture problems. *J. Mech. Phys. Solids* 43 (11), 1791–1824.
- Johnson, E., 1990. On the initiation of unidirectional slip. *Geophys. J. Int.* 101, 125–132.
- Johnson, E., 1992. Process region changes for rapidly propagating cracks. *Int. J. Fract.* 55, 47–63.
- Morrissey, J.W., Geubelle, P.H., 1997. A numerical scheme for mode III dynamic fracture problems. *Int. J. Numer. Methods Engng.* 40, 1181–1196.
- Needleman, A., 1999. An analysis of intersonic crack growth under shear loading. *ASME J. Appl. Mech.* 66, 847–857.

- Olsen, K.B., Madariaga, R., Archuleta, R.J., 1997. Three-dimensional dynamic simulation of the 1992 Landers earthquake. *Science* 278, 834–838.
- Ravi-Chandar, K., Lu, J., Yang, B., Zhu, Z., 2000. Failure mode transitions in polymers under high strain rate loading. *Int. J. Fract.* 101 (1–2), 33–72.
- Rosakis, A.J., Samudrala, O., Coker, D., 1999. Cracks faster than the shear wave speed. *Science* 284, 1337–1340.
- Washabaugh, P.D., Knauss, W.G., 1994. A reconciliation of dynamic crack velocity and Rayleigh wave speed in isotropic brittle solids. *Int. J. Fract.* 65 (2), 97–114.
- Zhu, Z., Ravi-Chandar, K., 1999. Experiments on dynamic shear crack propagation. *Proceedings of the International Conference on Advanced Techniques in Experiments*, pp. 395–402.